FULL PAPER

Holey Graphene Nanomanufacturing: Structure, Composition, and Electrochemical Properties

Yi Lin, Xiaogang Han, Caroline J. Campbell, Jae-Woo Kim, Bin Zhao, Wei Luo, Jiaqi Dai, Liangbing Hu,* and John W. Connell*

Topology is critical for properties and function of 2D nanomaterials. Membranes and films from 2D nanomaterials usually suffer from large tortuosity as a result from dense restacking of the nanosheets and thus have limited utility in applications such as electrodes for supercapacitor and batteries, which require ion transport through the nanosheet thickness. In comparison with conventional porous 2D nanomaterials, introducing holes through the nanosheets to create holey 2D nanomaterials with retention of the 2D-related properties is a more viable approach to improve molecular transport. Here, graphene is used as a model to study the fundamental structure-property relationship as a result from defect-enabled hole creation. Specifically, the correlation of electrochemical capacitive properties with structure and composition for holey graphene materials is prepared using a highly scalable controlled air oxidation process. The presence of holes on graphene sheets is not sufficient to account for the observed capacitance improvement. Rather, the improvement is achieved through the combination of an enhanced mesopore fraction with simultaneous oxygen doping while retaining the graphitic carbon network with minimal damage. The detailed understanding might be further applied to other 2D materials toward a broader range of both energy-related and other applications.

1. Introduction

2D atomic thick materials such as graphene, boron nitride, and MoS_2 have attracted much research interest recently.[1,2] However, the intrinsic properties of 2D materials leads to significant challenges including, for example, 1) restacking of the 2D nanosheets during film or composite formation; 2) difficulty for gases or solvents to escape the structure during manufacturing since individual flakes function as perfect barriers, which leads to a low packing density and poor flake–flake contact; 3) particularly for energy storages such as supercapacitors and batteries, high tortuosity for ion transport to access the surface of 2D materials. Researchers have been actively investigating porous structures based on 2D materials.[3–5] Although ions or gas species can be easily transported through the porous structures, the major disadvantage is the extremely low performance per volume.

Very recent studies on holey graphene (h-Graphene, sometimes also called "graphene nanomesh") have shown that introducing holes through the nanosheet basal plane could be an extremely efficient strategy to achieve much improved volumetric performance.[6,7] Different from the pore generation in which physical space is created between the intact nanosheets ("porous"), holey graphene is synthesized by chemically etching the nanosheet basal plane to form through-the-thickness holes ("holey"). Among a handful of available strategies, nanolithography methods[8–11] were used to prepare h-Graphene with highly periodic arrays of evenly distributed size holes, however these methods are not scalable. For large-scale preparation but with less precision in hole size/distribution, several methods were reported, such as etching with steam,[12] refluxing or sonicating with nitric acid,[13,14] chemical activation,[15] catalytic oxidation using metal or metal oxide nanoparticles,[16,17] enzymatic oxidation,[18] and photocatalytic oxidation,[19] among a few others.[3–5] The shared theme in the h-Graphene synthesis was the partial removal (mostly via oxidation) of the carbon atoms on the basal plane of graphene sheets.

Direct heating in air is one of the most facile and low-cost techniques to oxidize a given material. We recently demonstrated that directly heating of graphene sheets in air at controlled temperature and time resulted in h-Graphene with nanometer-sized holes of narrow size distributions.[6] The single-step air oxidation process is highly scalable, and the produced material could form robust and highly dense films that could be used as electrodes for ultracapacitors with high volumetric performance. However, the detailed structure-property

Dr. Y. Lin, C. J. Campbell, Dr. J.-W. Kim
National Institute of Aerospace
100 Exploration Way, Hampton, VA 23666, USA
E-mail: yi.lin-1@nasa.gov
Dr. Y. Lin
Department of Applied Science
The College of William and Mary
Williamsburg, VA 23185, USA
Dr. X. Han, B. Zhao, Dr. W. Luo, J. Dai, Prof. L. Hu
Department of Materials Science and Engineering
University of Maryland
College Park, MD 20742, USA
E-mail: binghu@umd.edu
Dr. J. W. Connell
Advanced Materials and Processing Branch
NASA Langley Research Center
Hampton, VA 23681-2199, USA

DOI: 10.1002/adfm.201500321

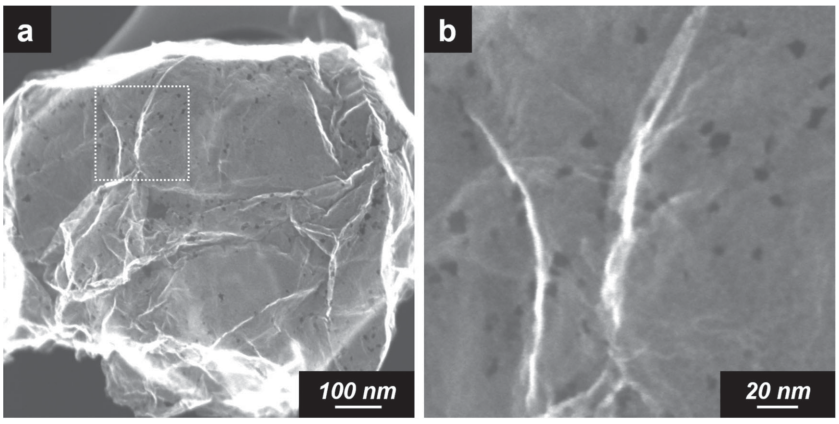

Figure 1. Typical SEM images of a) h-Graphene sample prepared at 430 °C/10 h. b) Enlargement of the dashed square in (a).

relationship of h-Graphene in related to the synthesis conditions remains to be fully understood.

In this article, we study the effects of the various synthesis parameters on the physical and chemical properties of the h-Graphene materials from controlled air oxidation. In particular, the intrinsic electrochemical capacitive properties were used as the main figure-of-merit in assessing the potential of this material in energy storage applications. We demonstrated that the holes and other characteristics of h-Graphene as a result of the air oxidation processes played different but key roles in the capacitive properties of the products. These results may be further extrapolated to benefit other applications of h-Graphene and may shed light on the synthesis and behavior of other holey 2D materials in general.

2. Results and Discussion

2.1. Manufacture of h-Graphene

The h-Graphene samples were prepared in a single-step air oxidation process by directly heating the starting graphene sample in static air at an elevated temperature in an open-ended tube furnace as previously described.[6] Unlike the starting graphene sheets, which were largely intact, the h-Graphene sheets exhibited through-the-thickness holes. For example, samples prepared at 430 °C and held for 10 h (hereinafter referred to as "430 °C/10 h") had hole diameters of ≈5–10 nm (**Figure 1**). The formation of the holes was due to the defect-rich regions on the graphene sheets being preferentially oxidized and gasified into CO and CO_2, leaving behind empty spaces (i.e., holes). As a result, despite the presence of holes on each individual sheet, h-Graphene samples prepared under these controlled conditions surprisingly exhibited equivalent or even somewhat improved graphitic crystallinity in comparison with the starting graphene as confirmed by Raman data (Figure S1, Supporting Information). For instance, the D-to-G ratios of the h-Graphene samples were slightly reduced, but their 2D peaks (≈2685 cm^{-1}; no meaningful shift) exhibited enhanced intensities and more defined line shapes.

2.2. Electrochemical Properties of h-Graphene

The electrochemical properties of h-Graphene sheets were characterized using a conventional 3-electrode setup with an aqueous KOH electrolyte (6.0 M). The CV plots at various scan rates from 10 to 1000 mV s^{-1} of the h-Graphene (430 °C/10 h) had near rectangle shapes (**Figure 2**a), indicating excellent electrical double-layer capacitive performance. Figure 2b,c compares the CV plots of two h-Graphene samples (430 °C/3 h and 430 °C/10 h) and the starting graphene at the same scan rate of 100 and 1000 mV s^{-1}, respectively. The enclosed areas of CV curves of h-Graphene samples were larger than that of the starting graphene, indicating higher relative capacitances. More specifically, the h-Graphene sample prepared at 430 °C/3 h exhibited only a marginal improvement in capacitance from the starting graphene, while that prepared at 430 °C/10 h had much more significant improvement. The capacitance improvement for the sample prepared at 430 °C/3 h were more obvious at higher scan rates (1000 mV s^{-1} in Figure 2c), indicating better performance retention upon rate increase.

Results from galvanostatic charge–discharge experiments conducted at different current densities were consistent with the CV data. For example, as shown in **Figure 3**a,b, the charge–discharge curves for the h-Graphene samples and the starting graphene were generally symmetrical (more so at higher current density), suggesting excellent reversible behavior. Specific gravimetric capacitance (C_m) values of these samples could be directly calculated from the discharge time in the galvanometric charge–discharge experiments: $C_m = I_m \Delta t/\Delta V$, where I_m is the current density; Δt is the discharge time; ΔV is the voltage window. The calculated C_m values of the h-Graphene samples and the starting graphene at different current densities are shown in Figure 3c. Similar to the results obtained from CV measurements (Figure 2), the capacitance values of the h-Graphene sample from shorter isothermal reaction hold times (430 °C/3 h) only had a small improvement from the starting graphene at lower current densities (e.g., 61 vs 59 F g^{-1} at 0.1 A g^{-1}), but retained their capacitance better than the starting graphene at higher current densities (e.g., 33 vs 25 F g^{-1} at 10 A g^{-1}). The h-Graphene sample from longer isothermal reaction times (430 °C/10 h) exhibited significant improvement of C_m values at all measured current densities, also with good capacitance retention at high current densities (102, 81, and 72 F g^{-1} at 0.1, 1, and 10 A g^{-1}, respectively).

The starting graphene exhibited excellent cycling performance as expected. As shown in Figure 3d, the sample retained ≈92% capacitance after 4200 cycles at 10 A g^{-1}, with most of the reduction occurring in the first 100 cycles. The cycling performance of h-Graphene samples was even better. For example, the C_m values of the h-Graphene sample (430 °C/10 h) exhibited very little change over similar number of cycles, with a total capacitance retention of ≈95%.

The above results demonstrated that the h-Graphene samples generally had enhanced rate performance than the starting

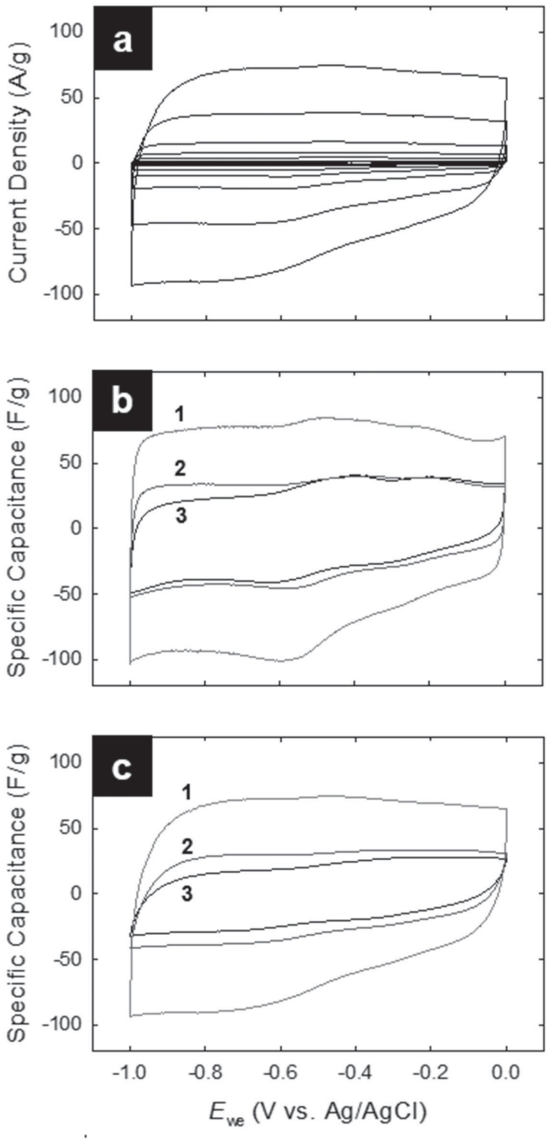

Figure 2. a) CV plots for a h-Graphene sample prepared at 430 °C/10 h at various scan rates (from inner to outer: 10, 20, 50, 100, 200, 500, 1000 mV s^{-1}). CV comparison at b) 100 mV s^{-1} and c) 1000 mV s^{-1} for the h-Graphene samples from 430 °C/10 h (**1**) and 430 °C/3 h (**2**) and the starting graphene sample (**3**). In (b,c), the *y*-axis was normalized to specific capacitance (C_m) by $C_m = I_m/(dV/dt)$, where I_m is the current density and dV/dt is the scan rate.

graphene with better capacitance retention at both higher voltage scan rates and current densities. The presence of holes on the graphitic plane likely helped the electrolyte ion transport and hence, more rapid formation of electric double-layer. However, the dramatic capacitance enhancement of the 430 °C/10 h sample over the 430 °C/3 h sample was intriguing.[20] The average hole diameters for the 430 °C/10 h and 430 °C/3 h h-Graphene samples were ≈8 and ≈5 nm, respectively,[6] both of which are far larger than the diameters of the electrolyte ions (hydrated K^+: 0.6; OH^-: 0.7 nm).[21] Therefore, it appears that the presence of holes alone on graphene sheets was insufficient to explain the observed significant capacitance improvement.

2.3. Correlation of h-Graphene Electrochemistry and Its Structure and Composition

In order to further examine the effect of holes from different synthetic conditions on the electrochemical performance of h-Graphene, another series of samples were prepared by heating the starting graphene sample in air at a ramp rate of ≈10 °C min^{-1} to various temperatures and all held for 10 h.[22] This set of experiments was designed such that the selected isothermal temperatures were near (both above and below) the main oxidative weight loss threshold of graphene (≈400–430 °C) as previously identified by TGA in a dynamic scan (10 °C min^{-1} in air).[6] Presumably, it might be preferable to retain as much of the graphene sheet crystallinity as possible, and selectively remove the defect sites to produce the holes. To achieve this, the heating conditions should ideally be kept above the oxidation threshold of defective carbons but below that of the graphitic carbons. The temperature window to achieve this was investigated experimentally by using the percentage weight retention (i.e., yield) of h-Graphene products after the various thermal treatment temperatures. As shown in **Figure 4**, when the isothermal temperature was in the range of 390–445 °C, the weights of various h-Graphene samples from 10 h heating only slightly decreased and consistently exhibited >85% in retention. The weight loss in this region could be readily attributed to defective carbon (Stage-I in Figure 4). This is further supported by both slightly reduced D-to-G ratio and the improved intensity and line shape of the 2D bands in Raman spectral results of the h-Graphene samples (Figure S2, Supporting Information). With 10 h heating duration, the threshold temperature for the subsequent main carbon loss was ≈445 °C. A slight temperature increase beyond this point resulted in significant further weight loss indicating degradation of the graphitic carbon (Stage-II in Figure 4). Despite the partial loss of graphitic carbon, the Raman spectra of h-Graphene samples obtained at 450 and 460 °C remained very similar to those from oxidation at lower temperatures, consistent with the notion that the remaining carbons in these samples still had good crystalline morphology.

Electron microscopy imaging (**Figure 5**) showed that the graphene sheets prepared at temperatures from 390–460 °C were all holey. The change in average hole diameters was nominal for h-Graphene samples prepared in the temperature region of defective carbon loss (<445 °C) (generally within the range of ≈5–10 nm). With more significant weight loss occurring above the thermal threshold conditions (>445 °C), the hole sizes of prepared h-Graphene increased. Meanwhile, the hole shape became much more irregular, likely due to anisotropic gasification of graphitic carbons from the hole edges. The sample prepared at 460 °C/10 h is a good example of the irregularly shaped holes with enlarged sizes that were observed (Figure 5f).

The specific capacitance performance of these h-Graphene samples showed a strong dependence on the synthesis temperature. As also shown in Figure 4, the C_m values measured from galvanostatic charge–discharge experiments at various current densities increased to a near maximum on the sample prepared at the graphitic carbon loss threshold (i.e., 445 °C/10 h). The rate performance results were consistent with previous observations where more enhancement at higher current

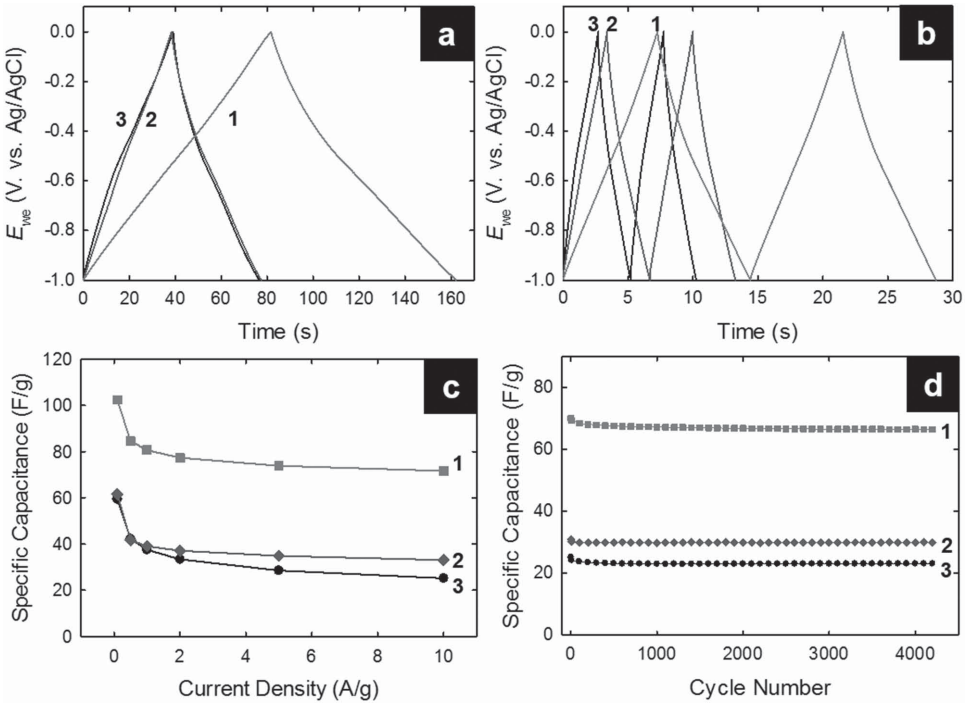

Figure 3. Galvanostatic charge–discharge curves at current densities of a) 1 A g^{-1} and b) 10 A g^{-1}; c) the dependence of specific capacitance on current density; and d) cycling performance at 10 A g^{-1} for the h-Graphene samples prepared at 430 °C/10 h (**1**) and 430 °C/3 h (**2**) and the starting graphene sample (**3**).

densities was found for all h-Graphene samples. The more striking observation was the dramatic capacitance improvement (almost doubled) when the isothermal temperature increased from 405 to 445 °C, while the hole sizes and the percentage weight retention values for these h-Graphene samples were nearly identical.

Apparently, other sample characteristics of the h-Graphene samples, in addition to the presence of holes, must have contributed to such a significant capacitance increase. Nitrogen adsorption–desorption and X-ray photoelectron spectroscopy (XPS) experiments were conducted to investigate the root cause for the observed behavior. As shown in **Figure 6**a, the isotherms of the h-Graphene samples appeared quite similar to the starting graphene in the low pressure region. As a result, the Brunauer–Emmett–Teller (BET) surface area values of the h-Graphene samples (from linear fit of data at P/P_0 ≈0.03–0.3) exhibited little to no improvement considering the error margin for the experiment (≈450–700 m^2 g^{-1}; Table S1, Supporting Information).[23] There was even a slight decrease of surface area values for h-Graphene samples obtained at lower temperatures, which might be due to that the selectively removed defect carbons had somewhat higher nitrogen adsorption capacity than the graphitic carbons. The total pore volume results obtained from the Barrett–Joyner–Halenda (BJH) method also exhibited little to no change. However, the difference came from the BJH pore distribution plots where the fraction of mesopores (centered at ≈12 nm) considerably increased in comparison with those of the micropores (centered at ≈1.9 nm) (Figure 6b). A pore distribution plot normalized at the micropore peak (Figure S3, Supporting Information) showed

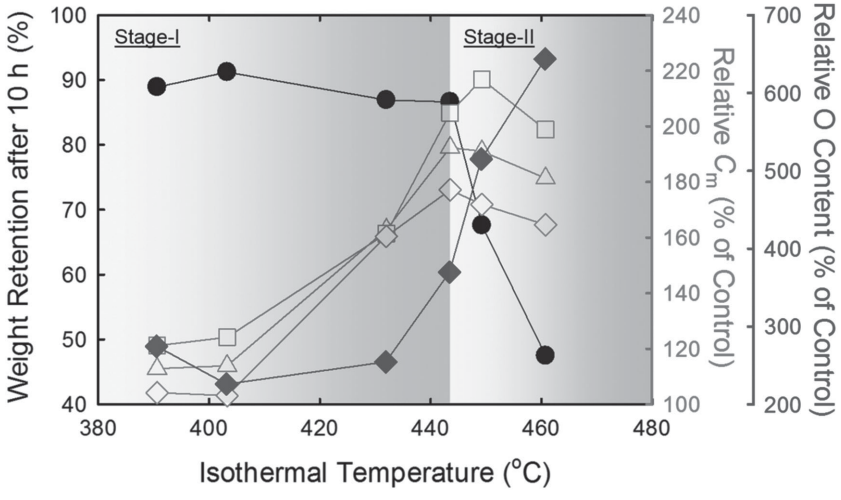

Figure 4. h-Graphene samples from 10 h air oxidation at different isothermal temperatures: the weight retention values (●); relative specific capacitance values (C_m) at different scan rates (◊: 0.5 A g^{-1}, Δ: 1 A g^{-1}, □: 10 A g^{-1}) in comparison with that of the starting graphene as control; and relative O contents from XPS survey results (♦) in comparison with that of the starting graphene as control. Stage-I and Stage-II temperature regions in h-Graphene preparation were assigned to the loss of defective and graphitic carbons, respectively.

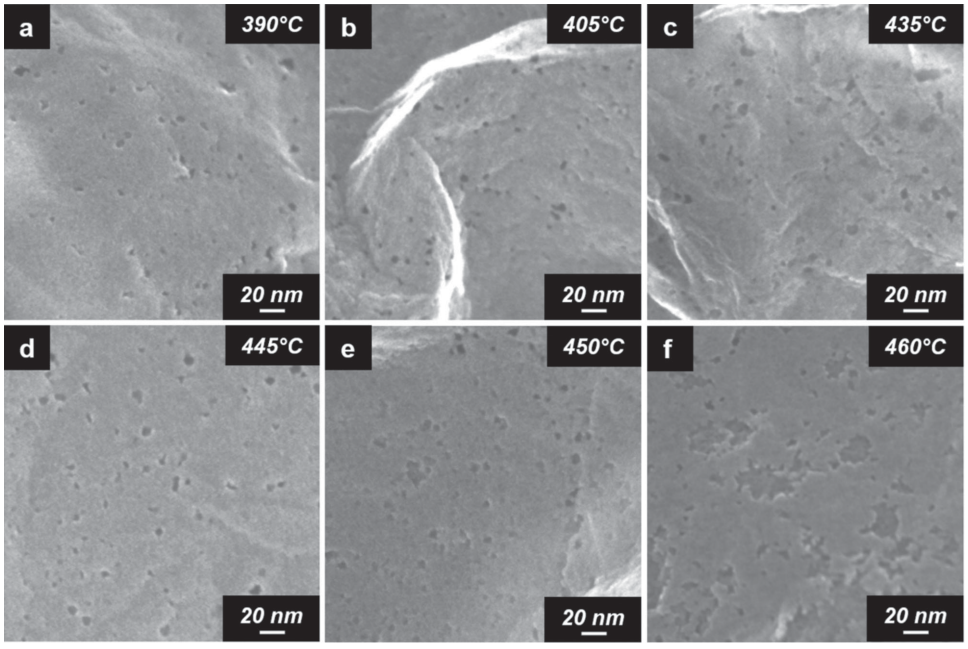

Figure 5. Typical SEM images of h-Graphene samples from 10 h air oxidation at different isothermal temperatures.

a progressive increase in mesopore fraction for the h-Graphene samples in comparison with the starting graphene. Therefore, in the defective carbon loss region, there was a strong correlation between the mesopore fraction and the capacitance performance. Meso-sized pores (2–50 nm) are known to be advantageous for electrochemical double layer formation in carbon-based electrodes.[24]

Mechanistically, it is likely that the locations of the micropores in the starting graphene were associated with defects, where the holes were preferentially formed upon oxidation. The formation of through-the-thickness holes with defective carbon gasification enlarged the micropores in the bulk solid sample, resulted in distinct reduction in micropore population and increased fraction of mesopores. Prolonged oxidation continued to improve the fraction of mesopores beyond the threshold of graphitic carbon loss, which caused more carbon gasification and thus even higher fraction of mesopores despite overall slightly changed total surface area. It is likely that the observed improved electrochemical rate performance with the presence of holes as discussed in previous sections is directly associated with the presence of mesopores, which happened to be colocated with the holes.

XPS survey data suggested that the oxygen contents for the h-Graphene samples (also plotted in Figure 4) were generally improved even for those obtained from lower isothermal temperatures (<410 °C; from 1.2% of starting graphene to ≈2.5%–3%; also see **Table 1** footnote). Interestingly, the most significant increase of oxygen content started at ≈430 °C, a temperature lower than the threshold of graphitic carbon gasification but in close coincidence with the threshold of capacitance improvement. High-resolution XPS scans of C and O signals revealed more details on the chemical composition of h-Graphene. There was no significant difference in the line shapes of the C-1*s* spectra of the h-Graphene samples and the starting graphene (Figure 6c), consistent with the notion that the graphitic structure was mostly preserved in h-Graphene. Detailed deconvoluted data (Table 1; Figure S4a–d, Supporting Information) showed the increase of various oxygen containing functional groups, especially the higher valence species (COOR), for h-Graphene in comparison with the starting graphene. The data also suggests that the h-Graphene samples from the defective carbon loss region were of very similar compositions, while there was a rather prominent increase of all oxygen containing functional groups when the reaction temperature was increased to 445 °C, the identified threshold of graphitic carbon loss.

In the O-1*s* region (Figure 6d), the intensities of the overall signals were significantly increased for the h-Graphene samples, consistent with the increased O content from the survey data mentioned above. The deconvoluted O-1*s* data (Table 1 and Figure S4e–h, Supporting Information) showed enhanced fraction of oxygen with higher carbon oxidation state (C=O at 533.5 eV vs C–O at 531.6 eV), consistent with the C-1*s* data. There were also components at even higher binding energies (≈536 and ≈538 eV), which were essentially absent in the starting graphene sample and progressively increased with the isothermal reaction temperature. Compared with the starting graphene, the new structure motifs in h-Graphene were holes. Therefore, these components were likely associated with oxygen atoms that were doped at or near the hole edges in the h-Graphene structure.

The increase of both mesopore fractions and oxygen species around the hole edges for the h-Graphene samples thus likely both contributed to the observed improvement of specific capacitance. When the heating was carried out in the temperature range where graphitic carbon loss occurs, both the mesopore fraction (Figure 6b) and the oxygen content (Table 1 and Figure 6d) continued to increase. However, the capacitive performance of h-Graphene samples reached a maximum,

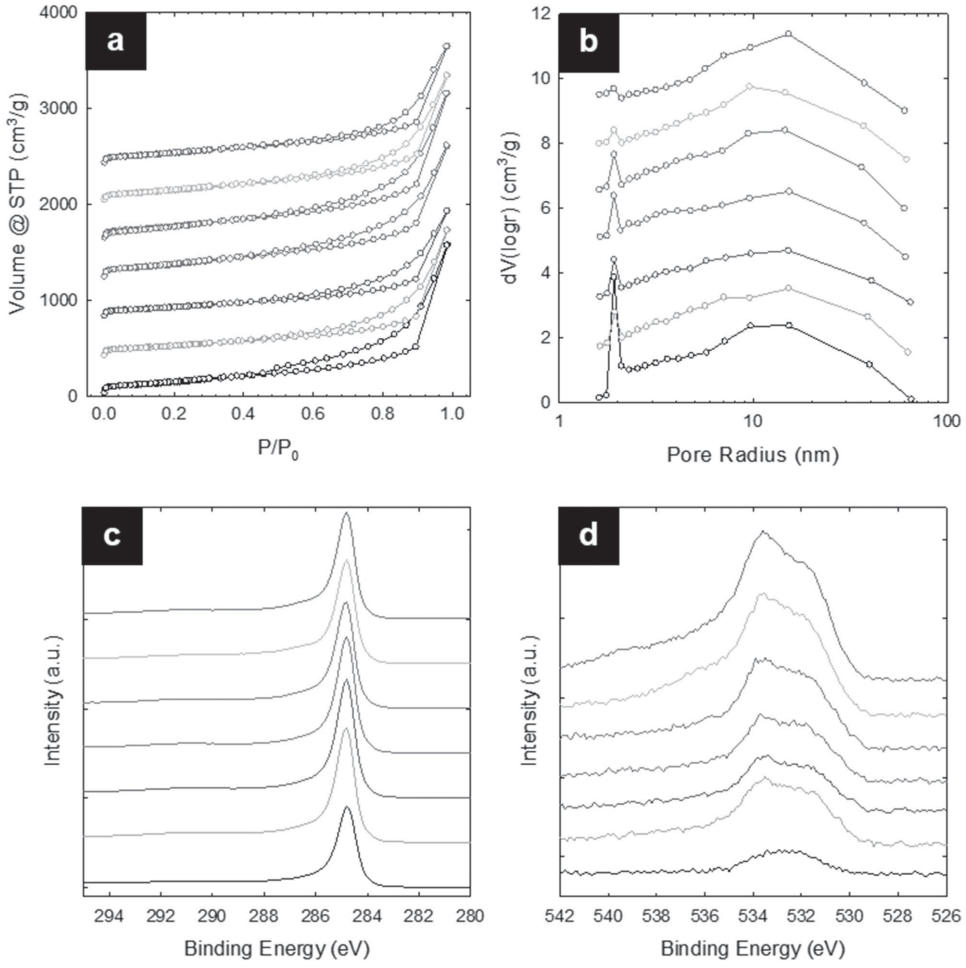

Figure 6. a) Nitrogen adsorption/desorption isotherms, b) BJH pore distribution, c) C-1*s*, and d) O-1*s* XPS spectra for the starting graphene (bottom most) and h-Graphene samples from 10 h air oxidation at different isothermal temperatures (for remaining traces from bottom to top: 390, 405, 435, 445, 450, 460 °C).

Table 1. XPS deconvolution data in the C-1*s* and O-1*s* regions for h-Graphene samples from 10 h air oxidation at different isothermal temperatures in comparison with that of the starting graphene.

Fitted peaks	Binding energy [eV]	Area [%]						
		G	h-Graphene (10 h air oxidation)					
			395 °C	405 °C	435 °C	445 °C	450 °C	460 °C
From C-1s								
sp^2	284.8	74.9	70	70.7	69.7	68.4	65.4	67
C-OR	286.4	8.2	10.3	9.8	10.5	11.5	13.2	12.6
C=O	288	3.2	3.8	3.9	3.7	4.2	6	4
COOR	289.3	1	1.3	1.2	1.2	1.6	1.7	1.8
From O-1s[a)]								
O-C	531.6	51.1	38.4	37.9	36.8	39.2	34.7	33. 9
O=C	533.6	45.4	46.8	47.2	44.2	48.2	44.6	44.3
Doped O 1	536–536.5	3.5	9.4	10.5	11.6	9.5	15.5	13.8
Doped O 2	538.2–539.2	–	5.4	4.4	7.4	3.1	5.2	8

[a)]The oxygen contents for the h-Graphene samples were 3.1 (395 °C), 2.6 (405 °C), 3.5 (435 °C), 4.2 (445 °C), 6.3 (450 °C), and 7.7% (460 °C), respectively, in comparison with 1.2% for the starting graphene sample.

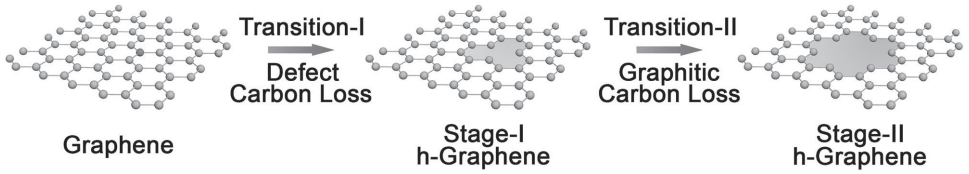

Scheme 1. The different formation stages of h-Graphene from controlled air oxidation.

plateaued and then began to exhibit signs of reduction, as shown in Figure 4. Apparently, the loss of too much graphitic carbon negatively affected the capacitive performance despite the positive effects from mesopore formation and oxygen doping. Clearly, there is a fine balance of chemical and morphological features that contribute to optimizing the capacitive performance of h-Graphene-based electrodes.

2.4. Formation Mechanism of h-Graphene

The above results suggested two main stages with two transition thresholds in the h-Graphene synthesis (**Scheme 1**). The first transition threshold is the gasification of defect carbons to generate holes, which leads to "Stage-I" h-Graphene that is structurally and chemically very similar to the starting graphene. The mesopore fraction and oxygen content continue to increase with the elevated reaction temperature until the second transition threshold, where the graphitic carbons start to gasify due to over-oxidation. The "Stage-II" h-Graphene has holes with larger sizes but reduced graphitic integrity. Fine tuning of air oxidation conditions may yield h-Graphene with desirable combination of crystallinity, mesopore fraction, as well as oxygen content. It is thus apparent that, in order to achieve optimal electrochemical capacitive performance, it is preferable to obtain h-Graphene with maximal carbon yield at the second transition threshold in the air oxidation process. For the h-Graphene samples obtained at the same temperature but with different heating durations (using a different tube furnace)[22] discussed in the earlier section of this work, a revisit on our prior nitrogen adsorption–desorption and XPS data[6] showed consistency with the above conclusions. With weight retention of ≈90% and ≈75%, the h-Graphene samples prepared at 430 °C/3 h and 430 °C/10 h could thus be categorized into Stage-I and Stage-II h-Graphene, respectively. It is important to emphasize that the temperature readings from different tube furnaces did not exactly match because of heating zone and other variations, making it critical to use the weight retention values as a more direct guidance. Nevertheless, the relatively narrow reaction (temperature and duration) window needed to achieve optimum capacitive performance speaks to the criticality of having high fidelity and accurate control of the synthetic process.

3. Conclusion

In summary, h-Graphene from controlled air oxidation exhibited through-the-thickness holes and enhanced electrochemical capacitive properties in comparison with the starting graphene material. The physical presence of holes benefited the rate performance in electrochemical processes of h-Graphene in general. However, the presence of holes alone was not sufficient to improve capacitance values. This improvement was only observed for h-Graphene samples prepared near or slightly above the temperature associated with graphitic carbon loss threshold. These h-Graphene samples contained enhanced mesopore fraction and oxygen doping most likely around the hole edges. The reported results shed light on the continued optimization of the h-Graphene materials from this facile and scalable process for the design and fabrication of electrode architectures to be used in ultracapacitors and batteries with superior gravimetric and volumetric performances. h-Graphene materials with tuned oxidation extent might also be used in other applications such as gas or ion separation that may have different requirements for physical, morphological, and chemical structures of graphene sheets. We envision that similar partial etching strategy could be generally applied to other 2D materials for holey 2D nanosheets. This unique subcategory of 2D materials might find broad applications in not only energy research, but also electronics, sensing, catalysis, and molecular transport and separation, and so forth.

4. Experimental Section

Materials: Graphene powder (Vor-X; grade: reduced 070; lot: BK-77x) was provided by Vorbeck Materials. Potassium hydroxide (KOH) was purchased from Fisher Scientific. Nafion solutions (5%, Type DE-521, Lot No.: SGA03–004) were purchased from Fuel Cell Store. All materials, solvents, and chemicals were used as-received. For preparation of h-Graphene, the starting graphene powder was placed in an alumina crucible and heated in static air with an open-ended tube furnace at a ramp rate of 10 °C min^{-1} and held isothermally at the set temperature for a given period of time to yield h-Graphene. The tube furnaces used included a single-zone furnace (Thermolyne Model 21100; manual temperature controller) and a dual-zone furnace (MTI Corporation OTF-1200X-80-II; automatic temperature controller). Reaction conditions varied slightly due to the different furnaces used because of dynamic heating conditions, dimension, and volume of heating zone, and air flow. All reaction temperatures were calibrated using an external temperature calibrator.

Measurements: Scanning electron microscopy (SEM) images were acquired using a Hitachi S-5200 field emission SEM (FE-SEM) system at an acceleration voltage of 30 kV. Raman spectra were acquired with an excitation wavelength of 532 nm on a Thermo-Nicolet-Almega Dispersive Raman Spectrometer. X-ray photoelectron spectroscopy (XPS) data were collected on a Kratos Axis 165 X-ray photoelectron spectrometer operating in hybrid mode using monochromatic Al Kα X-rays (1486.7 eV). Brunauer–Emmett–Teller (BET) surface area values and Barrett–Joyner–Halenda (BJH) pore characteristics were obtained from nitrogen adsorption–desorption isotherms collected using a Quantachrome Nova 2200e Surface Area and Pore Size Analyzer system.

Electrochemical Measurements: The electrochemical measurements were conducted on a Bio-Logic VMP3 electrochemical station. The 3-electrode tests were carried out with Ag/AgCl electrode (saturated with 3.5 M KCl) as the reference electrode and Pt wire as the counter electrode. The electrolyte solution (6.0 M KOH) was purged with argon for at least 20 min before use. To prepare a working electrode for the 3-electrode tests, the material of interest was first dispersed in a diluted Nafion solution (water : ethanol : as-received Nafion solution = 80 : 16 : 4 in volume) via ≈30 min bath sonication to form a dispersion with concentration of 1.0 mg mL^{-1}. A 10 µL drop of the dispersion (thus 10 µg of electrode material) was carefully placed onto a glassy carbon electrode (3 mm in diameter) followed by drying in a convection oven at 80 °C.

Supporting Information

Supporting Information is available from the Wiley Online Library or from the author.

Acknowledgements

The authors would like to thank M. Funk, L. Garcia, P. Tiemsin, and C. Chamberlain for experimental assistance. Y.L. acknowledges the financial support from the Leading Edge Aeronautics Research for NASA (LEARN) program (Grant No. NNX13AB88A). L.H. gratefully acknowledge the support from NSF-CBET (Grant Nos. 1335944 and 1335979), respectively. C.J.C. was a Langley Aerospace Research Summer Scholars (LARSS) Program scholar supported by LEARN.

Received: January 26, 2015
Revised: March 16, 2015
Published online: April 7, 2015

[1] M. J. Allen, V. C. Tung, R. B. Kaner, *Chem. Rev.* **2010**, *110*, 132.
[2] M. Xu, T. Liang, M. Shi, H. Chen, *Chem. Rev.* **2013**, *113*, 3766.
[3] L. Jiang, Z. Fan, *Nanoscale* **2014**, *6*, 1922.
[4] S. Han, D. Wu, S. Li, F. Zhang, X. Feng, *Adv. Mater.* **2014**, *26*, 849.
[5] J. Yang, M. Ma, L. Li, Y. Zhang, W. Huang, X. Dong, *Nanoscale* **2014**, *6*, 13301.
[6] X. Han, M. R. Funk, F. Shen, Y.-C. Chen, Y. Li, C. J. Campbell, J. Dai, X. Yang, J.-W. Kim, Y. Liao, J. W. Connell, V. Barone, Z. Chen, Y. Lin, L. Hu, *ACS Nano* **2014**, *8*, 8255.
[7] Y. Xu, Z. Lin, X. Zhong, X. Huang, N. O. Weiss, Y. Huang, X. Duan, *Nat. Commun.* **2014**, *5*, 4554.
[8] J. Bai, X. Zhong, S. Jiang, Y. Huang, X. Duan, *Nat. Nanotechnol.* **2010**, *5*, 190.
[9] X. Liang, Y. S. Jung, S. Wu, A. Ismach, D. L. Olynick, S. Cabrini, J. Bokor, *Nano Lett.* **2010**, *10*, 2454.
[10] A. Sinitskii, J. M. Tour, *J. Am. Chem. Soc.* **2010**, *132*, 14730.
[11] M. Wang, L. Fu, L. Gan, C. Zhang, M. Rummeli, A. Bachmatiuk, K. Huang, Y. Fang, Z. Liu, *Sci. Rep.* **2013**, *3*, 1238.
[12] T. H. Han, Y.-K. Huang, A. T. L. Tan, V. P. Dravid, J. Huang, *J. Am. Chem. Soc.* **2011**, *133*, 15264.
[13] X. Zhao, C. M. Hayner, M. C. Kung, H. H. Kung, *ACS Nano* **2011**, *5*, 8739.
[14] X. Wang, L. Jiao, K. Sheng, C. Li, L. Dai, G. Shi, *Sci. Rep.* **2013**, *3*, 1996.
[15] Y. Zhu, S. Murali, M. D. Stoller, K. J. Ganesh, W. Cai, P. J. Ferreira, A. Pirkle, R. M. Wallace, K. A. Cychosz, M. Thommes, D. Su, E. A. Stach, R. S. Ruoff, *Science* **2011**, *332*, 1537.
[16] Y. Lin, K. A. Watson, J.-W. Kim, D. W. Baggett, D. C. Working, J. W. Connell, *Nanoscale* **2013**, *5*, 7814.
[17] Y. Zhao, C. Hu, L. Song, L. Wang, G. Shi, L. Dai, L. Qu, *Energy Environ. Sci.* **2014**, *7*, 1913.
[18] G. P. Kotchey, G. A. Hasan, A. A. Kapralov, S. H. Ha, K. Kim, A. A. Shvedova, V. E. Kagan, A. Star, *Acc. Chem. Res.* **2012**, *45*, 1770.
[19] J. G. Radich, P. V. Kamat, *ACS Nano* **2013**, *7*, 5546.
[20] A similar relative enhancement factor was observed for C_m of h-Graphene versus starting graphene with 0.5 M H_2SO_4 as the electrolyte (Figure S5, Supporting Information), but that in an ionic liquid electrolyte was much less (<15%).[6] The latter could be attributed to both the bulky sizes of the ionic liquid electrolyte ions and less pronounced effect of oxygen doping in ion liquid versus aqueous electrolytes.
[21] J. Kielland, *J. Am. Chem. Soc.* **1937**, *59*, 1675.
[22] The temperature-dependent series of samples were conducted on a different tube furnace (MTI Corporation OTF-1200X-80-II; no thermal block used) from the time-dependent series discussed in the earlier sections of this manuscript (Thermolyne Model 21100; no thermal block used). Despite careful cross-calibration, there were still slight temperature differences (≈10–15 °C) in order to achieve the same carbon yield.
[23] Because of the low densities of the materials, each nitrogen adsorption–desorption experiment was conducted on only ≈10–20 mg of a given sample that could be fit in the sample bulb. The error margin for the measured absolute values from multiple experiments was thus found to be as large as 5%–10% even with the same calibrated sample bulb. However, the shapes of BJH pore distribution plots were highly repeatable despite the absolute pore volume differences in multiple experiments.
[24] P. Simon, Y. Gogotsi, *Acc. Chem. Res.* **2013**, *46*, 1094.